Jurnal Teknologi

Full Paper

EFFECT OF SENSOR ROTATION ON ASSESSMENT OF BENDER ELEMENT APPARATUS

Badee Alshameri[a*], Aziman Madun[b], Ismail Bakar[c], Edy Tonnizam Mohamad[d]

[a]Yemen Company for Investment in Oil and Minerals-YICOM, Sana'a, Yemen
[b]Faculty of Civil and Environmental Engineering, Universiti Tun Hussein Onn Malaysia, 86400 Parit Raja, Batu Pahat, Johor, Malaysia
[c]RECESS, Faculty of Civil and Environmental Engineering Universiti Tun Hussein Onn Malaysia, 86400 Parit Raja, Batu Pahat, Johor, Malaysia
[d]Geoengineering and Geohazard Research Group, Department of Geotechnics and Transportaion, Faculty of Civil Engineering, Universiti Tekhologi Malaysia, 81310 UTM Johor Bahru, Johor, Malaysia

Article history
Received
3 August 2015
Received in revised form
31 August 2015
Accepted
23 September 2015

*Corresponding author
badee.alshameri@yahoo.com

Graphical abstract

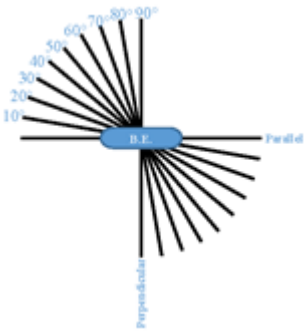

Abstract

The bender element is one of the most useful geophysical tools used in the laboratory to measure soil dynamics properties in a non-destructive way. However, inconsistent testing procedures may produce unrepeatable test results. Therefore, understanding the effect of the sensor rotation between the source and receiver position is crucial. This effect was evaluated using polystyrene material, which was unchanged throughout the period of testing. With sensor rotation angle starting from 0^0 to 90^0, the P-wave and S-wave velocities were calculated using five methods (Visual, First-peak, Maximum-peak, CC_{excel} and CC_{GDS}). The cross-correlation methods are used in two ways; by using normalized cross-correlation in Excel (knowned as CC_{excel}) and by using GDS (Geotechnical Digital Systems Company for supplying Geotechnical instrument) bender element analysis tool BEAT (knowned as CC_{GDS}). The results show that the Visual and First-peak methods gave a consistent wave velocity compared to the three other methods. In addition, both calculation methods were not significantly affected by increasing the sensor rotation angles. However, the Maximum-peak showed significant effect when the sensor rotation angle was above 20^0. The same issue was recognized for both cross-correlation methods when the sensor rotation angle was above 50^0. Moreover, the results from damping-slope indicated low effects for increasing the sensor rotation at P-wave and S-wave with sample thickness of 62.58 mm and 88.97 mm respectively (with an average damping-slope of about 3.5^0). In addition, the effect of the sensor rotation became more obvious at P-wave and S-wave with sample thickness of 88.97 mm and 62.58 mm respectively (with variation in the damping-slope 0.4^0 to 41.2^0).

Keywords: Bender element, procedure limitations, rotations, arrival time, cross-correlation, Damping-slope

Abstrak

Elemen Bender merupakan salah satu alat geofizik yang paling berguna di makmal untuk mengukur ciri-ciri dinamik tanah dengan cara yang tidak merosakkan. Walau bagaimanapun, ketiadaan prosedur ujian yang konsisten telah menyebabkan hasil ujian tidak dapat diulangi. Oleh itu, memahami kesan putaran sensor di antara sumber dan kedudukan penerima adalah penting. Kesan ini telah dinilai menggunakan bahan polistirena, yang tidak berubah sepanjang tempoh ujian. Dengan sudut putaran sensor bermula 0^0-90^0, kelajuan gelombang *P* dan *S* telah dikira dengan menggunakan lima kaedah (Visual, Puncak Pertama, Puncak Maksimum, CC_{excel} dan CC_{GDS}). Kaedah korelasi silang digunakan dalam dua cara; dengan menggunakan balas korelasi normal dalam excel (iaitu CC_{excel}) dan dengan menggunakan GDS (Geoteknik Sistem Digital Syarikat pembekal alat Geoteknik) alat analisis elemen Bender BEAT (iaitu CC_{GDS}). Hasil kajian menunjukkan bahawa kaedah Visual dan Puncak Pertama memberi halaju gelombang konsisten berbanding dengan lain-lain kaedah. Di samping itu, kedua-dua kaedah pengiraan tidak terjejas dengan ketara dengan meningkatkan sudut putaran sensor. Namun kaedah Puncak Maksimum menunjukkan kesan yang ketara apabila sudut putaran sensor lebih 20^0. Isu yang sama ditemui apabila kedua-dua kaedah korelasi silang apabila sudut putaran sensor melebihi 50^0. Selain itu, keputusan daripada cerun-redaman menunjukkan hampir tiada kesan putaran sensor terhadap gelombang *P* dan *S* dengan sampel ketebalan 62.58 mm dan 88.97 mm (dengan purata cerun-redaman kira-kira 3.5^0). Kesan putaran sensor menjadi lebih jelas bagi gelombang *P* dan *S* pada sampel berketebalan 88.97 mm dan 62.58 mm (dengan variasi dalam redaman-cerun 0.4^0-41.2^0).

Kata kunci: Bender elemen, batasan prosedur, putaran, masa perjalanan, balas korelasi, redaman-cerun

1.0 INTRODUCTION

One of the most useful geophysical tools in the laboratory is the bender element. Similar to other geophysical methods, the bender element is considered as a non-destructive method. However, many physical properties can be measured by using the bender element. Shear and Young's modulus can be measured via bender element by using equations 1 and 2:

$$E = V_p^2 \rho \quad (1)$$

$$G_0 = V_s^2 \rho \quad (2)$$

Where E, G_0 are the maximum Young's and shear modulus respectively in small stain range, V_p is compression wave velocity and V_s is shear wave velocity and ρ is bulk density.

Equations 1 and 2 show that the function of calculating the modulus depends on the measuring of compression and shear wave velocities (P-wave and S-wave). However, both compression and shear wave velocities can be measured by using the bender element tool [1-11].

The basic components of bender element consist of two plates of piezoceramic materials, which sandwich a thin plate of conductive metal. The function of bender element depends on the reaction and nature of piezoceramic material. This material is characterized by the dynamic electrical response. The piezoceramic material bends when the current flows through it and vice versa [1, 2, 3, 11, 12, 13]. In the bender element, the direction and polarization are the main parameters that control the function of this tool [1].

Figure 1 shows the different types of polarization and configurations of the bender element. In x-poled both of piezoceramic plates were placed to be bent (polarized) at the same direction. However, in y-poled both of piezoceramic plates were placed to be bent (polarized) in opposite directions. There are two types of bender element configurations, series and parallel. For series configuration, the positive wire connects to one plate and the negative wire connects to the other to become like the series and there is no connection to the middle thin metal plate. However, for parallel configuration, both of the piezoceramic plates are connected to the positive wire and the middle thin metal plate is connected to the negative wire. Due to the use of these configurations and polarizations, it can send and receive compression and shear waves without changing the wiring [2, 14] (Figure 1). However, in this paper, the effect of sensor rotation on the quality and procedure of bender element data was tested. Thus, the quality of bender element data and procedure can be improved.

2.0 METHODOLOGY AND PRINCIPLES

Due to difficulties in implementing this research in the soil samples using a short length of bender element (1 mm), the soil samples were replaced by polystyrene material. Polystyrene provides many advantages to

overcome the following trammels: (1) Provide good contact which can be difficult to achieve from soil samples. (2) Better control for the dimension of polystyrene sample compared to soil sample. (3) Control the moisture contact during the test (unlike in soil samples which will be subjected to change in moisture content during the period of testing) [2, 4]. Two polystyrene samples are used where the first sample (Figure 2a) has a dimension of 62.58 mm in height, 110.06 mm in length and 88.31 mm in width whereas the second one (Figure 2b) has a dimension of 88.47 mm in height, 100.94 mm in length and 62.02 mm in width.

Figure 3 shows a position sketch of BE top and bottom sensors in polystyrene samples. In parallel position (0^0), the top and bottom sensors of bender element are arranged on both sides of the sample until it is in the exact position and direction. Then, the top sensor of bender element is rotated by 10^0 and this continues until 90^0, which represent the perpendicular position of the top sensor of the bender element to the bottom sensor. The tests were conducted by changing the sensor positions starting from 0^0 (parallel) to 90^0 (perpendicular) as shown in Figure 3.

However, mono-frequency was used in this research (30 kHz) in order to avoid the near-field effect. The ratio of the wavelength to the wave path length was above 3 which is located in the safe zone so that it is not affected by the near-field effect [2, 8, 9, 15, 16, 17, 18, 19, 20]. On the other hand, sine waves were used to carry the waves [10, 21, 22, 23, 24].

Many researchers such as Viggiani and Atkinson [10], Yamashita et al. [25] and Arulnathan et al. [26] recommended measuring the wave velocity by accounting the wave path length from the tip of bender element source to the tip of bender element receiver. The calculations were according to the following equation:

$$V = \frac{L_{tt}}{t} \quad (3)$$

Where V is the wave velocity, L_{tt} is the wave path length from tip to tip and t is the arrival time (recorded time).

2.1 Methods to Calculate Wave Arrival Time and Damping-Slope

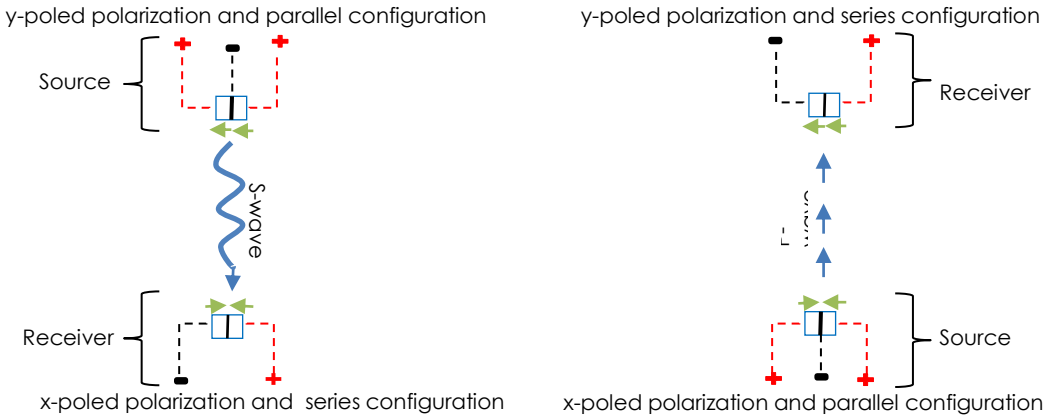

Figure 1 Bender element polarizations and configurations types

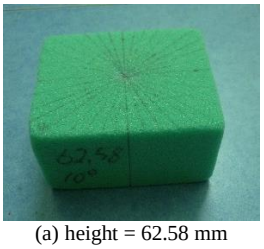

(a) height = 62.58 mm

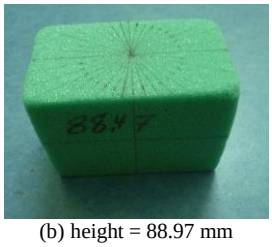

(b) height = 88.97 mm

Figure 2 Polystyrene samples

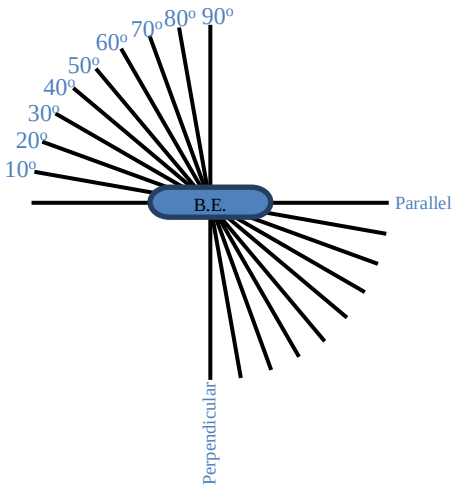

Figure 3 Position sketch of BE top and bottom sensors in polystyrene sample with rotation interval 10^0 starting from parallel (0^0) to perpendicular (90^0) to bender element pair

Generally, there are several methods to calculate first arrival wave time. However, in this research, five methods were used to calculate the arrival time (recorded time): (1) Visual results which were calculated directly from the screen software of the GDS bender element (version 1.5.3 was used in GDS bender element software) where GDS is Geotechnical Digital Systems Company for supplying geotechnical instruments. (2) First-peak by using excel Microsoft. (3) Maximum-peak also by using excel Microsoft. (4) Cross-correlation by using excel software CC_{excel}. (5) Cross-correlation by using GDS bender element analysis tools BEAT CC_{GDS} [28]. The next paragraph explains those methods.

The most well-known and simplest method to calculate the arrival time is First-peak, where the First-peak from source is recorded and the First-peak from the receiver is recorded. However, this method is less accurate than other methods such as cross-correlation methods. First-peak was used in both Visual and by using calculations in Excel. In Visual method, the detection of arrival time is faster than other methods; however, it has lower accuracy than other methods. In addition, for First-peak using Excel, (in related to the velocity calculations) both direct data and normalized data are used. In normalized data (normalized source and receiver), the data correlated to the maximum positive value. However, for damping calculations, only direct data was used [2, 10, 15, 25, 26, 27]

On the other hand, cross-correlation, which is an advanced method to calculate the arrival time of the waves, was used. In cross-correlation, two wave signals are compared to get the best similarity. The best fitting between any signals (from source and receiver) will be taken and time difference between the signals will be accounted as the travelling time [2, 10, 15, 19, 26, 28, 29].

Normalized cross-correlation equation (equation 4) was used to calculate the cross-correlation arrival time in Excel CC_{excel}. However, three modes of correlative points are used. From 4 through 5 to 6 correlative points are used to get the best fit, then the corresponding time (best fit between the source and receiver signals) was considered as the travel time.

$$\text{CC-norm}_{excel} = \frac{\sum_{T=0}^{T-1} X(T)Y(T)}{\sum_{T=0}^{T-1} X^2(T) \sum_{T=0}^{T-1} Y^2(T)} \qquad (4)$$

Where CC-norm_{excel} is the normalized correlation coefficient. T corresponds to the signal time record, Y(T) is source signal and X(T) is the receiver signal.

However, Rees et al. [28] described their new tools called "bender element analysis tools BEAT" which were used in this research to calculate the arrival time. However, this method was called, in this research, CC_{GDS} to identify it as the method programmed by the GDS company team (GDS is Geotechnical Digital Systems Company for supplying geotechnical instruments). The bender element analysis tools were designed to calculate the travel time in many ways including cross-correlation by using the following equation (equation 5):

$$CC_{xy}(t_s) = \frac{1}{T}\sum_{T=0}^{T-1} X(T)Y(T+t_s) \qquad (5)$$

Where $CCxy(t_s)$ is the time for maximum value of cross-correlation, t_s is the time shift for source signal, T corresponds to the signal time record, Y(T) is source signal and X(T) is the receiver signal [28].

In contrast, the damping-slop was calculated according to the difference between the maximum source and the maximum receiver amplitudes. However, to make the calculation of waves damping simple (i.e. not complicated) the difference in measurement units between the source and receiver signals was ignored (where the measurement units for the source signal was in volt (v) and the unit of the receiver was in millivolt (mv)).

3.0 RESULTS AND DISCUSSION

3.1 Velocities Results

Figure 4a and 4b show the plot of the results from the sensor rotation versus the P-wave and S-wave velocities respectively, which were calculated using different methods (Visual, first peak-to-first peak, Maximum-peak CC_{excel} and CC_{GDS}) for the sample with a thickness of 62.58 mm. Within the rotation angle from 0^0 to 80^0, Visual and First-peak show a similarity in the P-wave velocity with 522.2 m/s for Visual and 519.3 m/s for First-peak. However, when the rotation angle becomes equal to 90^0, the First-peak produced results equal to 454.3 m/s (Figure 4a). This is the same for S-wave velocities, which were within the range of 202.6 to 214.8 m /s for Visual and within the range of 201.9 to 213.8 m/s for First-peak (Figure 4b).

The Maximum-peak and cross-correlation for both CC_{excel} and CC_{GDS} show similarity in the results within rotation angle range between 0^0 to 20^0 with P-wave velocity equal to 227.2 m/s. Then the Maximum-peak started to give various values within the range of 213.8 to 519.3 m/s. However, within the rotation angle range between 0^0 to 80^0 both of the cross-correlation methods (CC_{excel} and CC_{GDS}) show a similarity in the results with a velocity equal to 227.2 m/s. Beside, when the rotation angle reaches 90^0, it shows an increase in the velocity which is 454.3 m/s.

3.2 Damping-Slope Results

Figure 5a and 5b show the plotting of the results from the sensor rotation versus the P-wave and S-wave damping, which were calculated using different sample thickness i.e. 62.58 mm and 88.47 mm respectively. In the sample with a thickness of 62.58 mm, the damping ratio for P-wave damping was in the range of 4.2 % and 9.5 %, while S-wave was in the

range of 1.6 % and 10.3 %. Moreover, for the sample with a thickness of 88.47 mm, the damping ratio of P-wave was in the range of 5.3 % and 51.2 %, while S-wave was in the range of 2.5 % and 7.3 %.

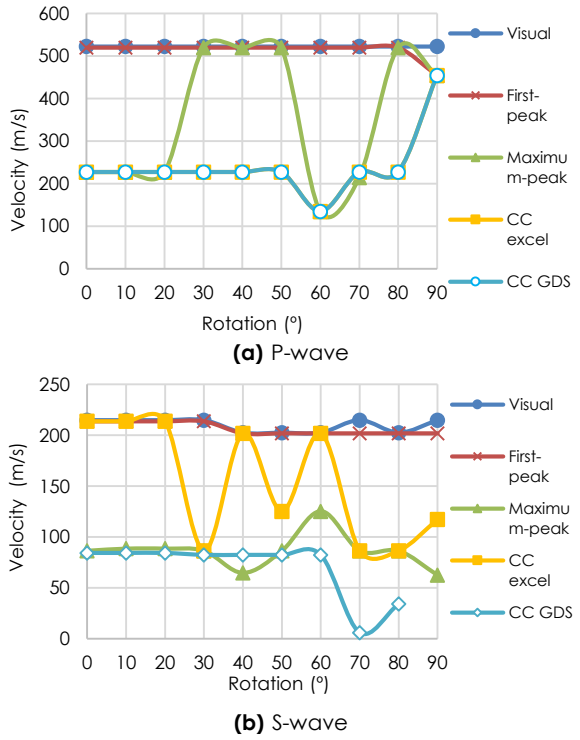

(a) P-wave

(b) S-wave

Figure 4 Calculated wave velocity at various rotation angle

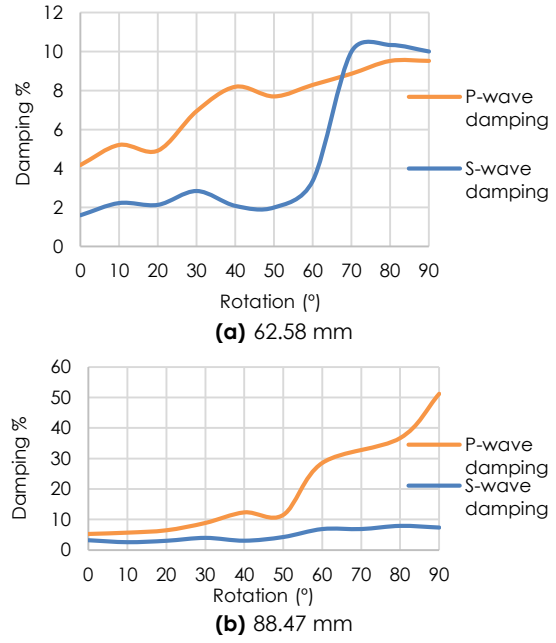

(a) 62.58 mm

(b) 88.47 mm

Figure 5 P-wave and S-wave damping at different sensor rotation

Figures 6a and 6b show the damping-slope for P-wave on the samples with a thickness of 62.58 mm and 88.47 mm respectively. The damping-slope for the sample with a thickness of 62.58 mm shows a smooth increase in the damping from 0^0 sensor rotation to 90^0 with a slope equal to 3.5^0 and R^2 equals to 0.9147. However, for the sample thickness of 88.47 mm, it was noted that the damping-slope can be divided into two zones. The first zone has a sensor rotation angle of 0^0 to 50^0. This zone shows an increase in the damping slightly with a slope equal to 8.7^0 and R^2 equal to 0.8867. The second zone has a sensor rotation angle above 50^0, where this zone shows rapid increase in the damping at slope 41.2^0 and R^2 equal to 0.8915.

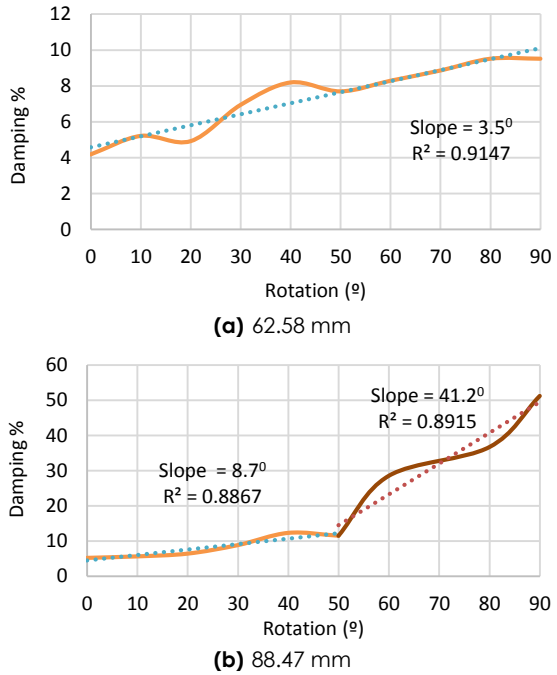

(a) 62.58 mm

(b) 88.47 mm

Figure 6 The coefficient of determination for the P-wave damping at different sensor rotation

Figure 7a and 7b show the damping-slope for S-wave on the samples with a thickness of 62.58 mm and 88.47 mm respectively. The damping results for the sample thickness of 62.58 mm show that the damping-slope can be divided into three zones. The first zone has a sensor rotation angle of 0^0 to 50^0, where this zone shows an increase in damping very slightly with a slope equal to 0.4^0 and R^2 equal to 0.4651. The second zone has a sensor rotation angle zone of 50^0 to 70^0. This zone shows rapid increase in the damping with a steep slope equal to 21.8^0 and R^2 equal to 0.8743. The third zone has a sensor rotation angle zone of 70^0 to 90^0. This zone shows almost no increase in the damping with a steep slope equal to 0^0 and R^2 equal to 0.9977.

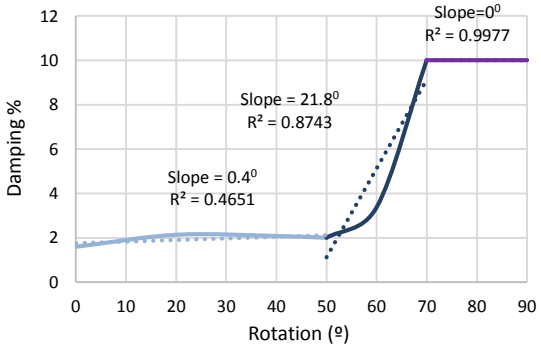

(a) 62.58 mm

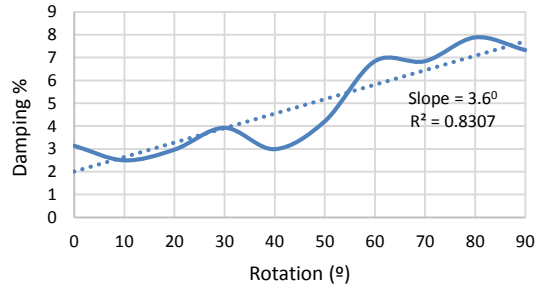

(b) 88.47 mm

Figure 7 The coefficient of determination for the S-wave damping at different sensor rotation

3.3 Discussion of Results

By referring to Figure 4, it has been noted that the calculations from Visual and First-peak always produce similar results for both P-wave and S-wave at all sensor rotation angles. Except for the sensor rotation angle 90^0 for First-peak, both Visual and First-peak methods were not affected by increasing the rotation angle. However, both methods showed a higher velocity (shorter time arrival) than the other three methods (Maximum-peak, CC_{excel} and CCG_{DS}). These results agree with those of previous researchers [2, 10, 15, 25, 26 and 30].

However, the results of P-wave velocity from Maximum-peak were subjected to variation when the sensor rotation angle increases above 20^0 while this variation started to appear after the sensor rotation was at 30^0 for S-wave velocity calculation. On the other hand, the results from both cross-correlations were subjected to variation when the sensor rotation angle was above 50^0 for P-wave velocity. For S-wave velocity, the cross-correlation showed differences in CC_{excel} and CC_{GDS}, which can be explained by choosing the correlative points in the two methods. The uncertainly in the results in Figure 4, can be considered as a guide for caution for the velocity calculation results when the bender element is subjected to sensor rotation angle higher than 20^0.

The differentials in the damping between the two samples can be explained via the loosing of wave energy due to the energy distribution as a function of geometry [31]. In addition, the damping results in Figures 6 and 7 show that the variation of damping-slope of P-wave is less affected when the thickness of the sample is relatively low compared to the variation of damping-slope of S-wave and vice versa. The P-wave damping-slope indicated a steep slope (41.2^0) when the sensor rotation is above 50^0 (in the second zone for the sample thickness of 88.47 mm). In addition, the S-wave damping-slope showed a steep slope (21.8^0) at zone 2 (at a sensor rotation of 50^0 to 70^0 for a sample thickness of 62.58 mm). Meanwhile, at zone 3 (at the sensor rotation between 70^0 and 90^0 for the sample thickness of 62.58 mm), the damping-slope becomes level. This is can be related to two facts: (1) The P-wave handle lower energy compare with the one at S-wave, which add extra effect for losing the energy with longer distance. (2) The nature of way of S-wave propagation and higher amount of energy which carried in S-wave cased high variation with increase the sensor rotation until specific point (at sensor rotation above 70^0) then no more variations in the damping. These results are in line with the results of other researchers such as Jong-Sub and Santamarina [5] who tested using bender element and Karl et al. [32] who tested using seismic cone penetration test. However, Parolai et al. [33] who tested using vertical arrays of accelerometers in the borehole showed disagreement with these results.

4.0 CONCLUSION

From the research carried out, it can conclude the following issues:

1. The results show that similarity in the velocity calculation between the First-peak and Visual methods. There was less variation in the P-wave velocity (519.3 m/s for First-peak and 522.2 m/s for Visual) for the sensor rotation from 0^0 until 90^0.
2. Both of Visual and First-peak gave a higher velocity than other methods (Maximum-peak, CC_{excel} and CC_{GDS}).
3. Using First-peak and Visual analysis methods, show no significant effect on P-wave and S-wave velocity when the sensor rotation was increased. While the P-wave and S-wave velocities were affected by the rotation sensor above 20^0 for the method of Maximum-peak and CC_{excel}, and above 50^0 for the CC_{GDS} method.
4. The increasing of the sample thickness and the sensor rotation caused the variation in the damping-slope for P-wave. In contrast, the decreasing of the sample thickness and the sensor rotation caused the variation in the damping-slope for S-wave.

Acknowledgement

The authors of this paper wish to express thanks to the Ministry of Higher Education (MOHE), Malaysia, MTCP and Research Centre of Soft Soil (RECESS) at University Tun Hussein Onn Malaysia (UTHM) (grants Vot. U260 and MDR1320).

References

[1] Eseller-Bayat, E., Gokyer, S., Yegian, M. K., Deniz, R. O. and Alshawabkeh, A. 2013. Bender Elements and Bending Disks for Measurement of Shear and Compression Wave Velocities in Large Fully and Partially Saturated Sand Specimens. *ASTM Geotechnical Testing Journal*. 36(2):275-282.

[2] Leong, E.C., Cahyadi, J. and Rahardjo, H. 2009.Measuring Shear and Compression Wave Velocities of Soil Using Bender-Extender Elements. *Canadian Geotechnical Journal*. 46:792-812.

[3] Mohammad, R. 2008. Dynamic Properties of Compacted Soils Using Resonant Column with Self-Contained Bender Elements. ProQuest.

[4] Rio, J. F. M. E. 2006. Advances in Laboratory Geophysics Using Bender Elements (Doctoral Dissertation, University of London).

[5] Jong-Sub Lee and J. Carlos Santamarina. 2005. Bender Elements: Performance and Signal Interpretation. *Journal of Geotechnical and Geoenvironmental Engineering*. 131(9). September 1, 2005. ©ASCE, ISSN 1090 0241/2005/9-1063-1070.

[6] Christophe, D. Hocine, H. and Pierre-Yves, H. 2003. Characterization of Loire River Sand in the Small Strain Domain Using New Bender-Extender Elements. *16th ASCE Engineering Mechanics Conference*. July 16-18, 2003. University of Washington, Seattle, USA.

[7] Arulnathan, R., Boulanger, R. W., Kutter, B. L. and Sluis, W. K. 2000. New Tool for Shear Wave Velocity Measurements in Model Tests. *ASTM Geotechnical Testing Journal*. 23(4):444-453.

[8] Jovicic, V., Coop. M. R. and Simic, M. 1996. Objective Criteria for Determining Gmax from Bender Element Tests. Technical Note. *Geotechnique*. 46(2): 357-362.

[9] Brignoli, E. G. M., Gotti, M. and Stokoe, K. H. 1996. Measurement of Shear Waves in Laboratory Specimens by Means Of Piezoelectric Transducers. *ASTM Geotechnical Testing Journal*. 19(4): 384-397.

[10] Viggiani, G. and Atkinson, J. H. 1995a. Interpretation of Bender Element Tests, Technical Note. *Geotechnique*. 45(1): 149-154.

[11] Viggiani G. and Atkinson, J. H. 1995b. Stiffness of Fine-Grained Soil at Very Small Strains. *Geotechnique*. 45(2):249-265.

[12] Germano, C. 2003. Flexure Mode Piezoelectric Transducers. Audio and Electroacoustics. *IEEE Transactions on*. 19(1):6.

[13] Lawrence, F.V. 1965. Ultrasonic Shear Wave Velocity in Sand and Clay. Massachusetts Institute of Technology, Cambridge, Mass. Research Report R65-05.

[14] Lings, M. L. and Greening, P. D. 2001. A Novel Bender/Extender Element for Soil Testing, Technical Note. *Geotechnique*. 51(8):713-717.

[15] Leong, E.C., Yeo, S.H. and Rahardjo, H. 2005. Measuring Shear Wave Velocity Using Bender Elements. *Geotechnical Testing Journal*. 28(5):488-498.

[16] Wang, Y. H., Lo, K. F., Yan, W. M. and Dong, X. B. 2007. Measurement Biases in The Bender Element Test. *Journal of Geotechnical and Geoenvironmental Engineering*. 133(5): 564-574.

[17] Bashar Alramahi. 2007. *Characterization of Unsaturated Soils Using Elastic and Electromagnetic Waves*. Doctoral Dissertation, Department of Civil and Environmental Engineering, Louisiana State University.

[18] Arroyo, M., Wood, D. M. and Greening, P. D. 2003. Source Near-Field Effects and Pulse Tests in Soil Samples. *Géotechnique*. 53(3):337-345.

[19] Sa´nchez-Salinero, I., Roesset, J. M. and Stokoe, K. H. 1986. Analytical Studies of Body Wave Propagation and Attenuation, Geotechnical Engineering Report No GR86-15. Civil Engineering Department, University of Texas at Austin. 272 pages.

[20] Knox, D.P.; Stokoe, K.H. and Kopperman, S.E. 1982. Effect of State of Stress on Velocity of Low Amplitude Shear Wave Propagating Along Principal Stress Directions in Dry Sand. *Geotechnical Engineering Research Report GR* 82-23. University of Texas at Austin.

[21] Callisto, L. and Rampello, S. 2002. Shear Strength and Small-Strain Stiffness of a Natural Clay under General Stress Conditions. *Geotechnique*. 52(8):547-560.

[22] Pennington, D. S., Nash, D. F. and Lings, M. L. 2001. Horizontally Mounted Bender Elements for Measuring Anisotropic Shear Moduli in Triaxial Clay Specimens. *ASTM Geotechnical Testing Journal*. 24(2):133-144.

[23] Blewett, J., Blewett, I. J. and Woodward, P. K. 2000. Phase and Amplitude Responses Associated With The Measurement of Shear-Wave Velocity in Sand by Bender Elements. *Canadian Geotechnical Journal*. 37(6):1348-1357.

[24] Gajo, A., Fedel, A. and Mongiovi, L. 1997. Experimental Analysis ofthe Effects of Fluid-Solid Coupling on the Velocity of Elastic Waves in Saturated Porous Media. *Géotechnique*. 47(5):993-1008.

[25] Yamashita, S., Kawaguchi, T., Nakata, Y., MIKAML, T., Fujiwara, T. and Shibuya, S. 2009. Interpretation of International Parallel Test on the Measurement of Gmax Using Bender Elements. *Soils and Foundations*. 49(4):631-650.

[26] Arulnathan, R., Boulanger, R. W. and Riemer, M. F. 1998. Analysis of Bender Element Tests. *Geotechnical Testing Journal*. 21(2): 120-131.

[27] Zarar, M. M. J. 2014. Personal Communication. Center of Electromagnetic Compatibility EMC, Universiti Tun Hussein Onn Malaysia UTHM. Johor, Malaysia. April 10.

[28] Rees, S., Le Compte, A. and Snelling, K. 2013. A New Tool for the Automated Travel Time Analyses of Bender Element Tests. *Proceedings of the 18th International Conference on Soil Mechanics and Geotechnical Engineering*. Paris 2013.

[29] Fonseca, A. V., Ferreira, C. and Fahey, M. 2009. A Framework Interpreting Bender Element Tests, Combining Time-Domain and Frequency-Domain Methods. *Geotechnical Testing Journal*. 32(2):91-107.

[30] Yang, J. and Gu, X. Q. 2013. Shear Stiffness Of Granular Material At Small Strains: Does It Depend On Grain Size?. *Géotechnique*. 63(2) :165-179.

[31] Telford, W. M., Geldart, L. P. and Sheriff, R. E. 2001. Applied Geophysics. Second Edition. The Press Syndicate of The University Of Cambridge. ISBN 0 521 339383.

[32] Karl, L., Haegeman, W. and Degrande, G. 2006. Determination of the Material Damping Ratio and the Shear Wave Velocity with the Seismic Cone Penetration Test. *Soil Dynamics and Earthquake Engineering*. 26(12):1111-1126.

[33] Parolai, S., Bindi, D., Ansal, A., Kurtulus, A., Strollo, A. and Zschau, J. 2010. Determination of Shallow S-Wave Attenuation by Down-Hole Waveform Deconvolution: A Case Study in Istanbul (Turkey). *Geophysical Journal International*. 181(2):1147-1158.